Analyst

PAPER

View Article Online
View Journal | View Issue

Cite this: *Analyst*, 2014, **139**, 3629

An efficient nanomaterial-based electrochemical biosensor for sensitive recognition of drug-resistant leukemia cells

Shaolian Zhang, Lu Zhang, Xi Zhang, Peihui Yang* and Jiye Cai

A novel electrochemical cytosensor was developed for the fast and high-sensitivity recognition of drug-resistant leukemia K562/ADM cells based on the P-glycoprotein (P-gp) expression level on a cell membrane. The nanocomposite interface of the gold nanoparticles/polyaniline nanofibers (AuNPs/PANI-NF) was chosen to design the biosensor for electrochemical detection. Au/PANI-NF-based cytosensors coated with anti-P-glycoprotein (anti-P-gp) molecules could provide a biomimetic interface for the immunosensing of cell surface P-glycoprotein, and thus could capture the over-expression P-gp cells. Transmission electron microscopy (TEM) indicated that the gold nanoparticles were uniformly anchored along the structure of the PANI-NF surface, displaying fibrillar morphology with a diameter of ~70 nm, and atomic force microscopy (AFM) further presented the morphology of the nanocomposite film. Owing to the high affinity of anti-P-gp for leukemia K562/ADM cells of the propounded sensing platform, the proposed biosensor exhibited excellent analytical performance for leukemia K562/ADM cells, ranging from 1.6×10^2 to 1.6×10^6 cells per mL with a detection limit of 80 cells per mL. Recovery experiments indicated that the sensitivity reported here is suitable for practical application. The cell surface P-gp expression level was analysed by flow cytometric experiments, which confirmed the above recognized result. This strategy is also a cost-effective and convenient operation, implying great promise for the sensitive recognition of cancer cells and cell surface receptors; thus, it is helpful in cancer diagnosis.

Received 4th March 2014
Accepted 6th May 2014

DOI: 10.1039/c4an00420e

www.rsc.org/analyst

1. Introduction

The efficient diagnosis and therapy of cancers have been hot topics in clinical and biomedical areas. One mechanism for the failure of chemotherapy in cancer treatment is the over-expression of an energy-dependent transport protein named P-glycoprotein (P-gp) at the tumor cell surface.[1] P-glycoprotein (P-gp, 150–170 kDa), a membrane transporter encoded by the MDR1 gene in human cells, comprises two nucleotide-binding and two membrane-spanning domains, acts as an energy-dependent pump that reduces intracellular drug concentrations below therapeutically effective levels.[2] In view of the importance of cell surface P-glycoprotein, a reliable and convenient method for recognizing drug-resistant cells *via* P-glycoprotein may help improve the diagnosis and treatment of cancer. Conventional methods such as flow cytometry,[3] immunohistochemistry,[4] ELISA,[5] and fluorescence[6] are widely utilized as analytical techniques for P-gp detection. Although these approaches have been used in some specific systems, most of them often have multi steps and are time-consuming or require highly technical skills and relatively sophisticated instrumentation. The development of a simple and convenient approach for cancer cell detection has received more and more interest.

Recently, electrochemical methods have been applied in cancer cell detection with the benefits of being simple, rapid, and convenient.[7–12] Zhang *et al.*[13] developed an electrochemical platform for the selective detection of apoptotic cells based on a SiO_2@QDs-ConA nanoprobe. Liu *et al.*[14] reported the detection of tumor cells based on the interaction between CdSe/ZnS quantum dots-labeled folic acids and folate receptors on the tumor cells. Zhu *et al.*[15] developed a novel electrochemical platform for the sensitive and selective detection of Michigan cancer foundation-7 human breast cancer cells based on aptamer–cell–aptamer sandwich architecture. Zheng *et al.*[16] reported nanoarchitectured electrochemical cytosensors for the selective detection of leukemia cells and quantitative evaluation of death receptor expression on cell surfaces. Most of the reported strategies could provide only qualitative tests or need long preparation time and more reaction steps or show undesirable biocompatibility. In recent years, an electrochemical strategy for improving the biocompatibility of a biosensor based on the interface of gold nanoparticles/polylactide nanocomposites has been reported.[17] However, the characterization of nanocomposite interface and the sensitivity of the biosensor were limited. Nevertheless, electrochemical cytosensors are still in the development phase, the key is to immobilize the

Department of Chemistry, Jinan University, Guangzhou 510632, People's Republic of China. E-mail: typh@jnu.edu.cn; zhangshaolian1990@163.com; Fax: +86-20-85223569; Tel: +86-20-85223569

recognition elements onto the electrode to provide sites of molecular recognition, but efficient immobilization is always a challenge; thus, a prominent underlying substrate is impending.

Nowadays, nanomaterial-based sensor interfaces are constructed for the electrochemical monitoring of cancer cells,[18–21] and the biofunctionalization of nanomaterials was the critical step in the preparation of nanomaterial-based biosensors. Polyaniline nanofibers (PANI-NFs) appear to be more attractive than carbon nanotubes as PANI-NFs show unique merits of large surface area, high conductivity, and the presence of many microgaps existing between the nanofibers and positive charges on the surface, which could absorb the negatively charged material, which had caused widespread concern.[22–26] Lower cytotoxicity and better biocompatibility of PANI-NFs make them suitable to construct biosensors.[27–29] Moreover, the presence of nitrogen atoms in PANI-NFs efficiently introduced chemically active sites and anchored metal nanoparticles.[30,31] In fact, gold nanoparticles (AuNPs), which possess good electronic properties and stability in immobilized living cells, were functionally fabricated as nanocomposites.[32–36] The effective immobilization of the cells can be achieved by AuNPs/PANI-NF nanocomposites.[18,37]

In this work, a novel electrochemical biosensor was constructed for K562/ADM cell recognition based on AuNPs/PANI-NF nanocomposites, which was used as an immobilization scaffold of anti-P-gp molecules to prepare sensitive immunosensors. PANI-NFs, AuNPs and anti-P-gp were employed to construct biosensors on glassy carbon electrodes (GCEs) *via* layer-by-layer assembly (Scheme 1). The novel anti-P-gp-functionalized cytosensors allowed for electrochemical impedance spectroscopic measurements evaluating the amount of K562/ADM cells. Multiple techniques including cyclic voltammetry (CV) and electrochemical impedance spectroscopy (EIS) were used to characterize the assembly process of the anti-P-gp-functionalized biosensor (anti-P-gp/AuNPs/PANI-NFs/GCE). Further, atomic force microscopy (AFM) and transmission electron microscopy (TEM) were used in the study of the nanostructured interface. Scanning electron microscopy (SEM) reveals the morphology of cells captured by the biosensor. This work presents the first attempt to use flow cytometry techniques to confirm recognition results, which demonstrate that different types of cancer cells could be distinctly detected by this new strategy with high sensitivity, reproducibility, rapidness and low cost.

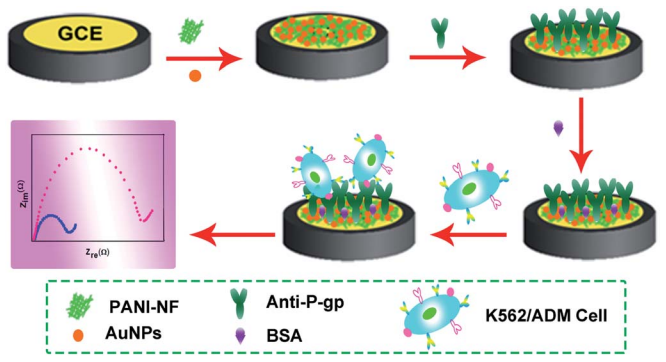

Scheme 1 Illustration of the preparation process of a label-free biosensor.

2. Experiment

2.1. Materials and reagents

P-glycoprotein antibodies were purchased from Beijing Biosynthesis Biotechnology Co., Ltd. (Beijing, China). Bovine serum albumin (BSA), hydrogen tetrachloroauric acid ($HAuCl_4 \cdot 3H_2O$), trisodium citrate, sodium borohydrate ($NaBH_4$) and $K_3[Fe(CN)_6]$ were obtained from Sigma-Aldrich Inc. (USA). AuNPs were prepared according to the literature by the citrate reduction method.[38] Polyaniline nanofibers (PANI-NFs) were synthesized according to the ref. 39 Phosphate buffer saline (PBS, 10 mM, pH 7.4) contained 136.7 mM NaCl, 2.7 mM KCl, 8.7 mM Na_2HPO_4, and 1.4 mM KH_2PO_4 were used as an incubation buffer. All other reagents were of analytical grade. All aqueous solutions were prepared using ultrapure water (≥18 MΩ, Milli-Q, Millipore).

2.2. Apparatus and characterizations

Electrochemical measurements, including electrochemical impedance spectroscopy (EIS) analysis and cyclic voltammograms (CV), were performed with a CHI 660 D electrochemical analyzer (CHI, USA). The three-electrode system was composed of a platinum wire as an auxiliary electrode, saturated calomel electrode as a reference electrode and GCE electrode as a working electrode. The nanostructure of nanocomposites was characterized by transmission electron microscopy (TEM, Philips) and an AutoProbe CP Research atomic force microscopy (AFM, Veeco, USA) in the tapping mode. Cell morphology at the nanoscale was visually characterized by scanning electron microscopy (SEM, Dutch). All of the images were smoothed by using Nanoscope software (IP 2.1) in order to remove the background noise at low frequency in the scanning direction. The flow cytometer was from obtained from Becton-Dickinson, USA.

2.3. Cell culture

Leukemia K562 cell lines obtained from a human epithelial carcinoma cell line were cultured in a flask in RPMI 1640 medium (GIBCO, USA) supplemented with 10% fetal calf serum (FCS, Sigma), penicillin (100 μg mL^{-1}), and streptomycin (100 μg mL^{-1}) at 37 °C in an incubator (5% CO_2, 37 °C). Cell counting was determined by the trypan blue exclusion method. Drug-resistant leukemia K562/ADM cells were obtained by incubating the cell in a culture medium in the presence of 1 μg mL^{-1} adriamycin (Sigma) for 3 h.

2.4. Preparation of biosensors

The glassy carbon electrode (GCE) was carefully polished by 0.3 μm and 0.05 μm alumina. Then, it was sonicated successively with distilled water and ethanol for 5 min until a mirror-like surface was obtained. Then, 10 μL of 2 mg mL^{-1} PANI-NF

suspension, dispersed in double-distilled water with the aid of ultrasonication, was dropped on the pretreated GCE surface and dried in a desiccator to obtain the PANI-NF/GCE, which was then immersed in a solution containing 2 mg mL^{-1} of AuNPs for 1 h and dried in a desiccator to obtain AuNPs/PANI-NFs/GCE. Then, 10 μL of 1 mg mL^{-1} anti-P-gp was immediately dropped on its surface and incubated at 37 °C for 2 h to yield the anti-P-gp/AuNPs/PANI-NFs/GCE. Following a rinse with 0.01 M PBS (pH 7.4), the modified electrode was soaked in 0.01 M PBS containing 0.5% BSA for 10 min to block the remaining active sites and eliminate the non-specific binding effect. After thorough washing with 0.01 M pH 7.4 PBS, the obtained anti-P-gp-functionalized biosensor (anti-P-gp/AuNPs/PANI-NFs/GCE) was stored at 4 °C. The preparation process of the modified electrode is shown in Scheme 1.

2.5. Analytical procedures by the electrochemical biosensor

CV was carried out in 5.0 mM $[Fe(CN)_6]^{3-/4-}$. EIS was carried out in the presence of 5.0 mM $K_3[Fe(CN)_6]$–$K_4[Fe(CN)_6]$ (1 : 1) mixture and 0.1 M KCl by applying an alternating current voltage with 5 mV amplitude in a frequency range from 0.1 Hz to 100 kHz. A suspension of K562/ADM cells or K562 cells at a given concentrations was dropped on the anti-P-gp-functionalized biosensor for cell capture at 37 °C for 2 h. After carefully washing with incubation buffer, the electrode was immersed in degassed PBS (0.01 M, pH 7.4) to remove cells without the specific identification of the interface. The specific identification and capture of K562/ADM and K562 cells on the biosensor interface were studied by EIS.

2.6. Flow cytometry analysis

The P-gp molecules expression on the K562/ADM cells and K562 cells surface was evaluated by flow cytometry. The cells were rinsed and dissolved with ice-cold PBS containing 1% BSA at a concentration of 1×10^6 cells per mL and incubated with 20 μL of FITC-labelled monoclonal anti-P-gp at 4 °C for 30 min in the dark. After incubation, cells were washed and resuspended in chilled PBS. The binding affinity of the FITC-labelled P-gp antibody was analysed using an FACSCalibur flow cytometer. Unlabeled cells were used as the negative control for the estimation of P-gp molecules expression.

3. Results and discussion

3.1. Characterization of the biosensor interface

TEM and AFM were used to investigate the biosensor interface. Fig. 1 depicted typical TEM micrographs of pure PANI-NFs, AuNPs, AuNPs/PANI-NFs and anti-P-gp/AuNPs/PANI-NFs. The superstructures of bamboo-like PANI-NFs were typically composed of nanofibers of about 50–80 nm in diameter (Fig. 1A), whereas AuNPs showed an average diameter of about 20 nm (Fig. 1B). AuNPs were homogeneously dispersed on the surface of PANI-NFs, forming a hybrid structure of AuNPs/PANI-NFs nanocomposites (Fig. 1C). Compared with PANI-NFs, AuNPs/PANI-NFs had a unique surface-protuberance-like hybrid nanostructure, which had a large ratio of surface active

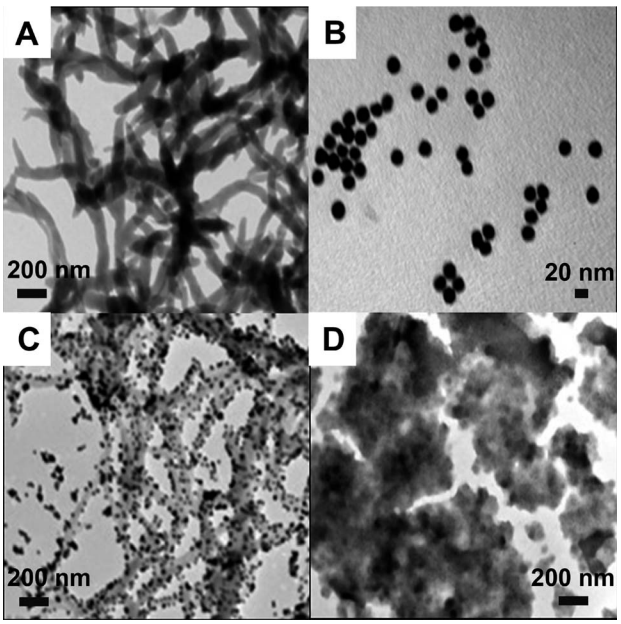

Fig. 1 TEM images of (A) PANI-NFs, (B) AuNPs (C) PANI-NFs/AuNPs, and (D) PANI-NFs/AuNPs/anti-P-gp-modified films.

groups to volume and appreciable integrity with no or little leakage of AuNPs. AuNPs were aggregated on the nanofiber surface, and such aggregation appeared to result from the chemical inertness of regular PANI-NFs. This result suggested a strong interaction between AuNPs and PANI-NFs, which might be caused by N-participation in their connection, a reaction that is similar to the case of immobilizing Ni, Cu and Pt nanoparticles on nitrogen-doped carbon nanotubes.[40–42] Additionally, the connection might be promoted further by electrostatic interactions between negatively charged AuNPs and positively charged PANI-NFs. Given that, AuNPs could function as an immobilized matrix and firmly bind antibodies (Fig. 1D) presumably through ionic interactions and other interactions between AuNPs and mercapto or primary amine groups of antibodies.[43] Au/PANI-NF nanocomposites appeared to offer a more homogenous surface for antibody conjugation, and subsequently cell loading. In fact, we found Au/PANI-NFs nanocomposites enhanced the reproducibility of the cytosensor assay and exhibited robust sensitivity for collecting signals.

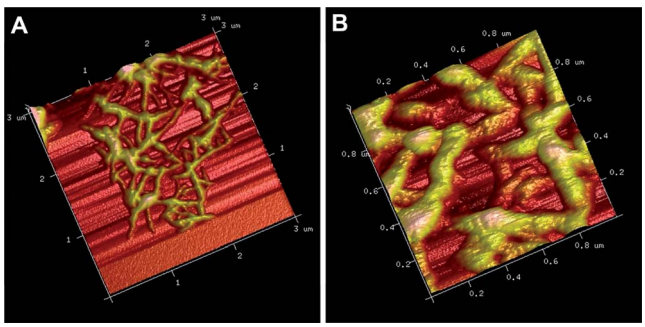

Fig. 2 AFM images of (A) PANI-NFs and (B) anti-P-gp/AuNP/PANI-NFs.

The surface topographies of PANI-NFs and anti-P-gp/AuNPs/PANI-NF films were analyzed by AFM, and the images are shown in Fig. 2A and B, respectively. Network-like structures can be found in Fig. 2A, which indicates the existence of PANI-NFs. After AuNPs and anti-P-gp were assembled onto the PANI-NF film as shown in Fig. 2B, obviously, the surface of anti-P-gp/AuNPs/PANI-NF films becomes smooth, dense and compact.

3.2. Electrochemical features of the biosensor

CV was applied to characterize the modified electrode. Fig. 3A presents the CVs of the electrode at every stage. As shown in Fig. 3A, compared with the bare GCE electrode (curve a), the peak currents increased after the binding of PANI-NFs (curve b); this might be due to the excellent redox activity of nanometer-sized polyaniline nanofibers, which played an important role similar to that of a conducting wire or electron-conducting tunnel. When AuNPs were conjugated to the PANI-NF surface, CVs of AuNPs/PANI-NFs/GCE exhibited increased redox peak currents (curve c), suggesting that AuNPs effectively promoted electron transfer. These results implicate that the conjugation between AuNPs and PANI-NFs was strong and that the leakage of AuNPs from the PANI-NF surface could be ignored. However, the peak currents decreased after the modified electrode was immersed in the solution of P-gp antibodies (curve d), which indicated that P-gp antibody had been immobilized on the electrode surface successfully. Subsequently, when the biosensor was incubated with K562/ADM cells, a dramatic decrease of the peak currents may be attributed to the captured cells (curve e), which can hinder the transmission of electrons toward the electrode surface.

When EIS measurements (Fig. 3B) were used to monitor the change in electron-transfer resistance (R_{et}) of $[Fe(CN)_6]^{3-/4-}$ as redox probes, the bare GCE showed low resistance (curve a). The subsequent assembly of the PANI-NF layer on the electrode surface facilitated interfacial electron transfer (curve b). The coating of AuNPs on PANI-NFs/GCE significantly facilitated interfacial electron transfer, exhibiting a straight line in the spectrum (curve c), demonstrating that Au/PANI-NF nanocomposites could improve the electrical connectivity of electrode, and thus significantly enhance detection sensitivity. After the electrode surface was coupled by anti-P-gp Ab molecules, and subsequently, blocked for non-specific binding by BSA, an increase in R_{et} was observed (curve d), indicating that Ab themselves acted as an inert electron- and a mass-transfer blocking layer. An interesting phenomenon can be observed in curve e: the diameter of the semicircular domain had an obvious increase when cells were decorated onto the anti-P-gp/AuNPs/PANI-NFs/GCE film (curve e). Because P-gp molecules were widely expressed on the K562/ADM cell surface, the R_{et} value implied that K562/ADM cells were successfully captured by the cytosensor. The highly conductive AuNPs and PANI-NF composite films could not only increase the surface area for cell capture but also greatly enhance electrical connectivity, which would improve the sensitivity of cell recognition.

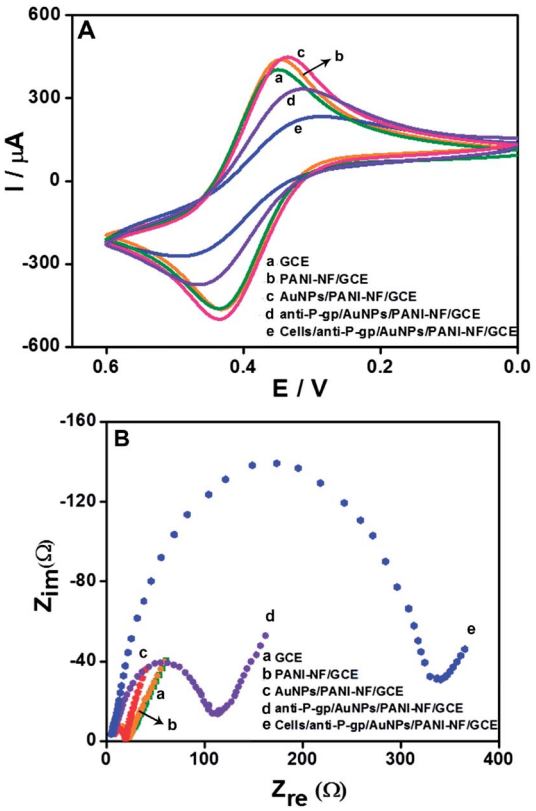

Fig. 3 CV(A) and EIS (B) values detected from (a) GCE, (b) AuNPs/PANI-NFs/GCE, (c) anti-P-gp/AuNPs/PANI-NFs/GCE, (K562/ADM cells)/anti-P-gp/AuNPs/PANI-NFs/GCE in 10 mM pH 7.4 phosphate buffered saline containing 0.1 M KCl, 5 mM $K_3[Fe(CN)_6]$ and 5 mM $K_4[Fe(CN)_6]$.

3.3. Recognize, distinguish K562 and K562/ADM cells

By investigating the specificity of the interfacial properties and the electrochemical behavior of the $[Fe(CN)_6]^{3-/4-}$ probe on the anti-P-gp-biosensor covered with the same concentration but different types of leukemia cells, EIS and flow cytometry techniques were applied in the recognition of the target cells. Owing to the good biocompatibility of AuNPs/PANI-NF composites, K562/ADM cancer cells could be specifically recognized by using antibody-conjugated biosensor targeting corresponding surface molecules.

As shown in Fig. 4A, EIS values of K562/ADM cells captured by the biosensor (curve a) were 3 times greater than those of K562 cell signals (curve b). This is due to the over-expression of P-gp protein molecules on the K562/ADM cell surface and then specific recognition by the biosensor; thus, the binding of cells to the anti-P-gp Ab molecule-functionalized biosensor further hindered the access of redox probes to the electrode, leading to a high R_{et} value. Interestingly, none or very low EIS signals were detected by the biosensor in the blank (curve b) or in presence of K562 cells (curve a). This might be due to the less expression of P-gp protein molecule on the K562 cell surface, P-gp antibody-functionalized sensor surface trapped less K562 cells, leading to low EIS signals. According to the remarkably different EIS signals of K562/ADM and K562 cells, these two types of cells could be accurately differentiated by this P-gp antibody-functionalized electrode interface.

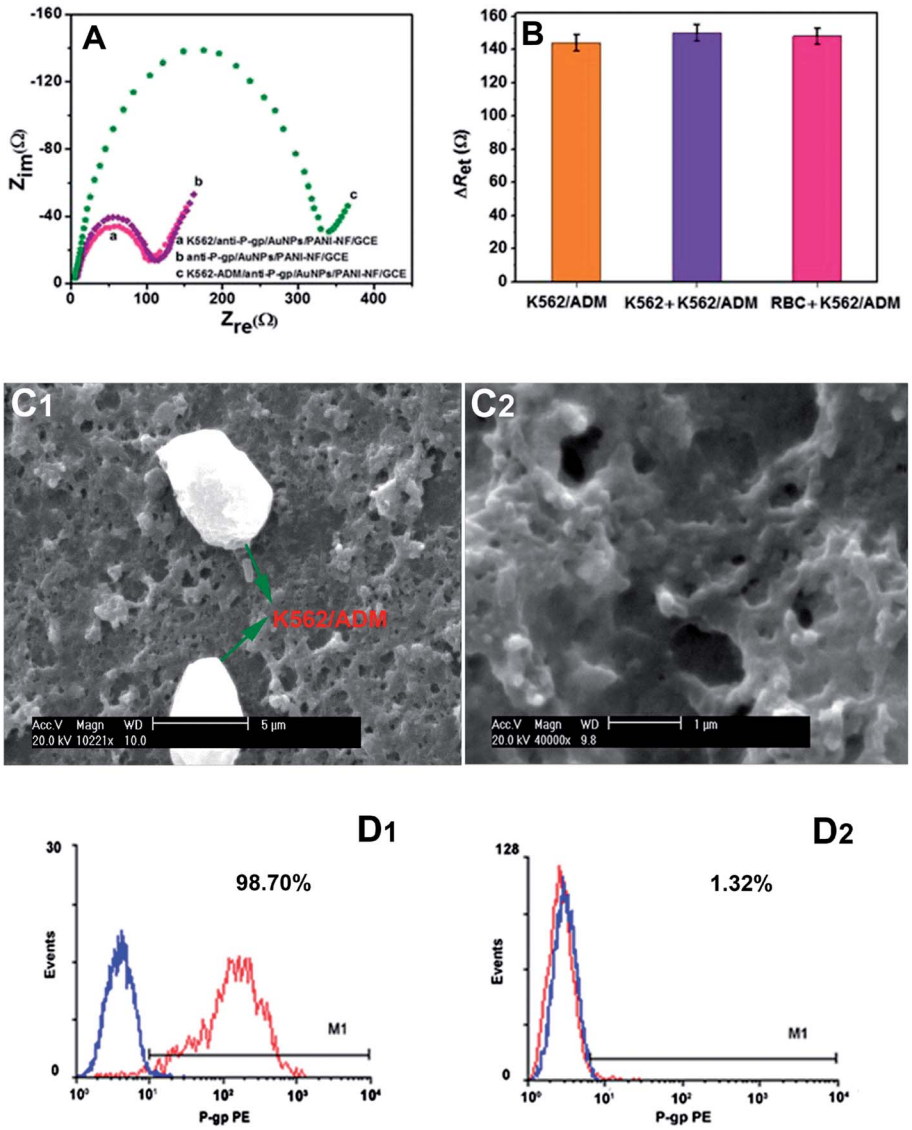

Fig. 4 EIS signals (A) obtained from (a) K562 cells/anti-P-gp/AuNPs/PANI-NFs/GCE, (b) anti-P-gp/AuNPs/PANI-NFs/GCE, (c) (K562/ADM cells)/anti-P-gp/AuNPs/PANI-NFs/GCE in 10 mM PBS (pH 7.4) containing a 0.1 M KCl solution, 5 mM $K_3[Fe(CN)_6]$ and a 5 mM $K_4[Fe(CN)_6]$ solution. (B) Specificity of the proposed cytosensing strategy. Error bars were the standard deviation of five replicate determinations. SEM images of the biosensor interface after recognizing cancer cells. (C_1) (K562/ADM cells)/anti-P-gp/AuNPs/PANI-NFs/GCE, (C_2) the K562 cells/anti-P-gp/AuNPs/PANI-NFs/GCE. Flow cytometric experiments analyse the expression level of P-gp on the cell surface. (D_1) K562/ADM cells, (D_2) K562 cells.

Different kinds of cells at the same concentration (1.0×10^4 cells per mL) were applied to further study the specificity of the proposed cytosensor for K562/ADM recognition. K562/ADM cell lines mixed with human K562 leukemic cells or human red blood cells (RBC) were incubated on the fabricated cytosensor for 2 h and rapidly detected by EIS. Meanwhile, K562/ADM cells were also incubated under the same experimental conditions as a control. As shown in Fig. 4B, no significant changes of EIS signals were found in comparison with the result obtained in the presence of K562/ADM only, suggesting good specificity of the fabricated cytosensor.

From the SEM image shown in Fig. $4C_1$, K562/ADM cells were successfully captured on the biosensor surface, while K562 cells showed no adherence to the interface in Fig. $4C_2$. To examine our results, we also performed flow cytometry experiments, which can be used to analyse the P-gp expression level on the cell surface. Using the same calculation scale, K562/ADM cells showed an increased expression of P-gp up to 98.7% (Fig. $4D_1$), while K562 cells have a positive P-gp rate of 1.32% (Fig. $4D_2$), suggesting that the P-gp expression on K562/ADM cells and K562 cells represents a significant difference. This result supported the EIS performance and was also confirmed by SEM images.

3.4. K562/ADM cells detection

The concentration-dependent behavior of the impedance signal when drug-resistant leukemia K562/ADM cells were captured by the biosensor was investigated to evaluate the possibility of sensitively detecting the cells. As shown in Fig. 5, increases in the magnitude of ΔR_{et} correlated with the number of cells specifically

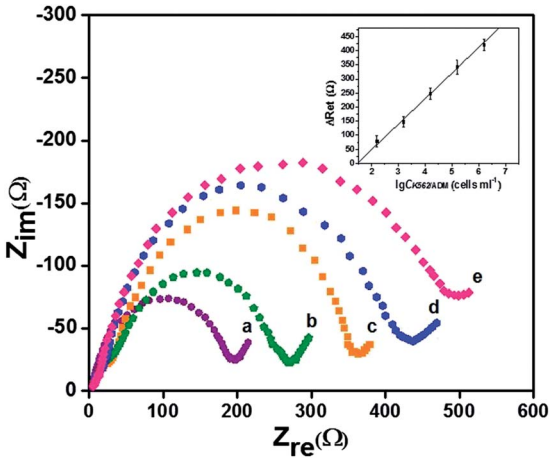

Fig. 5 EIS of anti-P-gp/AuNPs/PANI-NFs/GCE incubation in different concentrations of K562/ADM cell measured. (a) 1.6×10^2, (b) 1.6×10^3, (c) 1.6×10^4, (d) 1.6×10^5, (e) 1.6×10^6 cells per mL. Inset: linear relationship between electron transfer resistance (ΔR_{et}) and logarithm of K562/ADM cells concentration. The error bars represent the standard deviation of three independent measurements.

bound to the biosensor. The inset of Fig. 5 shows the linear relationship between the ΔR_{et} values and the logarithm of the K562/ADM cell concentration in the range from 1.6×10^2 cells per mL to 1.6×10^6 cells per mL. The regression equation was $\Delta R_{et} = 85.62 \log C - 118.3$ (C is in units of cells per mL) with a regression coefficient of 0.9949. The detection limit was 80 cells per mL ($S/N = 3$). This detection limit is lower than those of previously reported biosensors such as the electrochemical biosensor based on CdSe/ZnS quantum dots (QDs)-labeled folic acids (2000 cells per mL)[14] and the electrochemical biosensor based on aptamer–cell–aptamer sandwich architecture (100 cells per mL).[15] The factors that contributed significantly to sensitive K562/ADM cell detection were high specificity recognition and binding between the antibody-immobilized AuNPs/PANI-NF interface and P-gp over-expressed on the surface of the K562/ADM cell.

To evaluate whether the assay could be useful for actual sample, recovery experiments were performed to monitor ΔR_{et} after mixing two types of cells including 1000 cells per mL K562/ADM cells and different concentration of K562 cells. The concentration ratios ($C_{K562/ADM} : C_{K562}$) were 1 : 1, 1 : 5, 1 : 10, respectively. It was found that when the concentration of K562 cells was 10 000 cells per mL in the mixed-cell solution, the average ΔR_{et} values ($n = 3$) were 150 Ω, which was close to 144 Ω for 1000 cells per mL K562/ADM cells. Recovery experiments showed that recovery yields of the EIS assay from K562 cell samples spiked with K562/ADM cells present recoveries in the range from 96% to 107% with an average of 102%.

3.5. Reproducibility, stability and reusability of the cytosensor

The reproducibility of the biosensor for detecting K562/ADM cells was investigated. Under the optimization experiment condition, the constructed sensors were used to detect the electrochemical impedance values of 2000 cells per mL K562/ADM cells for 10 times, the R_{et} relative standard deviation (RSD) is only 2.1%. The results suggested that the biosensor exhibited acceptable reproducibility in its linear range. Furthermore, the storage stability of the biosensor was also studied. After stored at 4 °C in 10 mM PBS (pH 7.4) for 3 weeks, the biosensor showed that the average EIS value was 95.5% of the initial EIS value for 2000 cells per mL K562/ADM cells, showing good stability. The reusability of the sensor was investigated by using 0.2 M glycine–HCl at pH 2.2 for 0.5 h to rinse out the K562/ADM cells from the biosensor. This resulted in a complete release of K562/ADM cells, and glycine–HCl was then removed by treatment with PBS (pH 7.4). After re-exposure to K562/ADM cells, the modified electrode could again capture cells. After 5 cycles, the R_{et} values still remained 80%. The signal decrease can result from unavoidable contamination, desquamation of the film and denaturation of anti-P-gp. This result showed that the anti-P-gp-functionalized cytosensor could be regenerated with acceptable reusability. The above results showed that the anti-P-gp-functionalized cytosensor has good reproducibility, stability, and ease of regeneration; hence, this cytosensor is a potential candidate for recognition of cancer cells.

4. Conclusions

In summary, AuNPs/PANI-NF nanocomposites could efficiently immobilize anti-P-gp, and serve as electrochemical cytosensor interface. Our results suggest that this anti-P-gp-functionalized biosensor is simple, efficient and can be sensitive to the recognition of the drug-resistant leukemia K562/ADM cells, as well as quantitatively detect drug-resistant leukemia K562/ADM cells with a wide linear range and low detection limit. These findings possess potential application for developing versatile cytosensors for guiding the clinical evaluation of inflammation, infection or cancer.

Acknowledgements

This work was supported by grants from National Natural Science Foundation China (no. 21375048), the Major State Basic Research Development Program of China (973 Program) (no. 2010CB833603).

References

1 J. M. Norgaard and P. Hokland, *Int. J. Hematol.*, 2000, **72**, 290–297.
2 J. P. Marie and O. Legrand, in *Drug Resistance in Leukemia and Lymphoma III*, ed. G. J. L. Kaspers, R. Pieters and A. J. P. Veerman, 1999, vol. 457, pp. 1–9.
3 J. H. Ahn, G. H. Jang and M. Lee, *J. Cell. Physiol.*, 2013, **228**, 1496–1505.
4 C. Akfirat, X. T. Zhang, A. Ventura, D. Berel, M. E. Colangelo, C. K. Miranti, M. Krajewska, J. C. Reed, C. S. Higano, L. D. True, R. L. Vessella, C. Morrissey and B. S. Knudsen, *J. Pathol.*, 2013, **230**, 291–297.

5 D. Kuhnke, G. Jedlitschky, M. Grube, M. Krohn, M. Jucker, I. Mosyagin, I. Cascorbi, L. C. Walker, H. K. Kroemer, R. W. Warzok and S. Vogelgesang, *Brain Pathol.*, 2007, **17**, 347–353.
6 L. Tao, C. J. Song, Y. J. Sun, X. H. Li, Y. Y. Li, B. Q. Jin, Z. J. Zhang and K. Yang, *Anal. Chim. Acta*, 2013, **761**, 194–200.
7 C. Tlili, E. Sokullu, M. Safavieh, M. Tolba, M. U. Ahmed and M. Zourob, *Anal. Chem.*, 2013, **85**, 4893–4901.
8 D. D. Zhang, Y. M. Zhang, L. Zheng, Y. Z. Zhan and L. C. He, *Biosens. Bioelectron.*, 2013, **42**, 112–118.
9 H. L. Liu, Y. Y. Cui, P. Li, Y. M. Zhou, Y. Chen, Y. W. Tang and T. H. Lu, *Anal. Chim. Acta*, 2013, **776**, 24–30.
10 J. Y. Liu, Y. N. Qin, D. Li, T. S. Wang, Y. Q. Liu, J. Wang and E. K. Wang, *Biosens. Bioelectron.*, 2013, **41**, 436–441.
11 C. Hu, D.-P. Yang, Z. Wang, P. Huang, X. Wang, D. Chen, D. Cui, M. Yang and N. Jia, *Biosens. Bioelectron.*, 2013, **41**, 656–662.
12 C. Hu, D.-P. Yang, F. Zhu, F. Jiang, S. Shen and J. Zhang, *ACS Appl. Mater. Interfaces*, 2014, **6**, 4170–4178.
13 J.-J. Zhang, T.-T. Zheng, F.-F. Cheng, J.-R. Zhang and J.-J. Zhu, *Anal. Chem.*, 2011, **83**, 7902–7909.
14 Y. Liu, L. Zhu, J. Kong, P. Yang and B. Liu, *Electrochem. Commun.*, 2013, **33**, 59–62.
15 X. L. Zhu, J. H. Yang, M. Liu, Y. Wu, Z. M. Shen and G. X. Li, *Anal. Chim. Acta*, 2013, **764**, 59–63.
16 T. Zheng, J.-J. Fu, L. Hu, F. Qiu, M. Hu, J.-J. Zhu, Z.-C. Hua and H. Wang, *Anal. Chem.*, 2013, **85**, 5609–5616.
17 X. J. Wu, H. Jiang, J. S. Zheng, X. M. Wang, Z. Z. Gu and C. Chen, *J. Electroanal. Chem.*, 2011, **656**, 174–178.
18 H. Wang, H. H. Cai, L. Zhang, J. Cai, P. H. Yang and Z. W. Chen, *Biosens. Bioelectron.*, 2013, **50**, 167–173.
19 J. A. Barreto, W. O'Malley, M. Kubeil, B. Graham, H. Stephan and L. Spiccia, *Adv. Mater.*, 2011, **23**, H18–H40.
20 C. Hu, D.-P. Yang, Z. Wang, L. Yu, J. Zhang and N. Jia, *Anal. Chem.*, 2013, **85**, 5200–5206.
21 C. Hu, D.-P. Yang, K. Xu, H. Cao, B. Wu, D. Cui and N. Jia, *Anal. Chem.*, 2012, **84**, 10324–10331.
22 Q. Wu, Y. Xu, Z. Yao, A. Liu and G. Shi, *ACS Nano*, 2010, **4**, 1963–1970.
23 S. Singh, P. R. Solanki, M. K. Pandey and B. D. Malhotra, *Anal. Chim. Acta*, 2006, **568**, 126–132.
24 M. U. A. Prathap, B. Thakur, S. N. Sawant and R. Srivastava, *Colloids Surf., B*, 2012, **89**, 108–116.
25 R. Rawal, S. Chawla, T. Dahiya and C. S. Pundir, *Anal. Bioanal. Chem.*, 2011, **401**, 2599–2608.
26 H. Wang, T. Wang, Y.-X. Ye, Y.-X. Zhang, P.-H. Yang, H.-H. Cai and J.-Y. Cai, *Chin. J. Anal. Chem.*, 2012, **40**, 184–190.
27 F. Hu, S. Chen, C. Wang, R. Yuan, Y. Xiang and C. Wang, *Biosens. Bioelectron.*, 2012, **34**, 202–207.
28 E. Spain, R. Kojima, R. B. Kaner, G. G. Wallace, J. O'Grady, K. Lacey, T. Barry, T. E. Keyes and R. J. Forster, *Biosens. Bioelectron.*, 2011, **26**, 2613–2618.
29 D. Y. Zhai, B. R. Liu, Y. Shi, L. J. Pan, Y. Q. Wang, W. B. Li, R. Zhang and G. H. Yu, *ACS Nano*, 2013, **7**, 3540–3546.
30 J. Huang, S. Virji, B. H. Weiller and R. B. Kaner, *J. Am. Chem. Soc.*, 2003, **125**, 314–315.
31 X. Peng, L. Peng, C. Wu and Y. Xie, *Chem. Soc. Rev.*, 2014, **43**, 3303–3323.
32 J. Sharma, R. Chhabra, A. Cheng, J. Brownell, Y. Liu and H. Yan, *Science*, 2009, **323**, 112–116.
33 N. Xia, L. P. Zhang, G. F. Wang, Q. Q. Feng and L. Liu, *Biosens. Bioelectron.*, 2013, **47**, 461–466.
34 H. Song, Y. Ni and S. Kokot, *Anal. Chim. Acta*, 2013, **788**, 24–31.
35 B. Haghighi and M. A. Tabrizi, *Colloids Surf., B*, 2013, **103**, 566–571.
36 M. Yan, G. Q. Sun, F. Liu, J. J. Lu, J. H. Yu and X. R. Song, *Anal. Chim. Acta*, 2013, **798**, 33–39.
37 H. Zhang, R. Liu and J. Zheng, *Synth. Met.*, 2013, **167**, 5–9.
38 G. Frens, *Nature*, 1973, **241**, 20–22.
39 J. Huang and R. B. Kaner, *Angew. Chem.*, 2004, **116**, 5941–5945.
40 K. Ghosh, M. Kumar, T. Maruyama and Y. Ando, *J. Mater. Chem.*, 2010, **20**, 4128–4134.
41 M. Park, B.-H. Kim, S. Kim, D.-S. Han, G. Kim and K.-R. Lee, *Carbon*, 2011, **49**, 811–818.
42 W. H. Shin, H. M. Jeong, B. G. Kim, J. K. Kang and J. W. Choi, *Nano Lett.*, 2012, **12**, 2283–2288.
43 S. H. Yang, W. H. Shin, J. W. Lee, H. S. Kim, J. K. Kang and Y. K. Kim, *Appl. Phys. Lett.*, 2007, **90**, 013103.